

Multi Positive Contrastive Learning with Pose-Consistent Generated Images

Sho Inayoshi¹, Aji Resindra Widya¹, Satoshi Ozaki¹,
Junji Otsuka¹, and Takeshi Ohashi¹

Sony Group Corporation, Tokyo, Japan
{Sho.Inayoshi, Aji.Widya, Satoshi.Ozaki, Junji.Otsuka,
Takeshi.A.Ohashi}@sony.com

Abstract. Model pre-training has become essential in various recognition tasks. Meanwhile, with the remarkable advancements in image generation models, pre-training methods utilizing generated images have also emerged given their ability to produce unlimited training data. However, while existing methods utilizing generated images excel in classification, they fall short in more practical tasks, such as human pose estimation. In this paper, we have experimentally demonstrated it and propose the generation of visually distinct images with identical human poses. We then propose a novel multi-positive contrastive learning, which optimally utilize the previously generated images to learn structural features of the human body. We term the entire learning pipeline as GenPoCCL. Despite using only less than 1% amount of data compared to current state-of-the-art method, GenPoCCL captures structural features of the human body more effectively, surpassing existing methods in a variety of human-centric perception tasks.

Keywords: Self-supervised learning · Controllable image generation · Human-centric perception

1 Introduction

Model pre-training has become essential in various recognition tasks. Especially within human-centric perception tasks (*e.g.*, human pose estimation, person ReID, *etc.*), there is a movement towards leveraging a pre-trained model as a foundational framework. This approach is motivated by the extensive variety of tasks, each with substantial learning costs, and the demonstrated superior performance of such models [10, 15, 16, 36, 60, 64]. Recently, HAP [64] proposed to implicitly learn structural features of the human body, which has shown promising results. While pre-training shows promising results, it needs a huge amount of data. Hence, an increasing number of pre-training methods utilizing generated data have been proposed given their ability to produce unlimited training data [30, 61, 62].

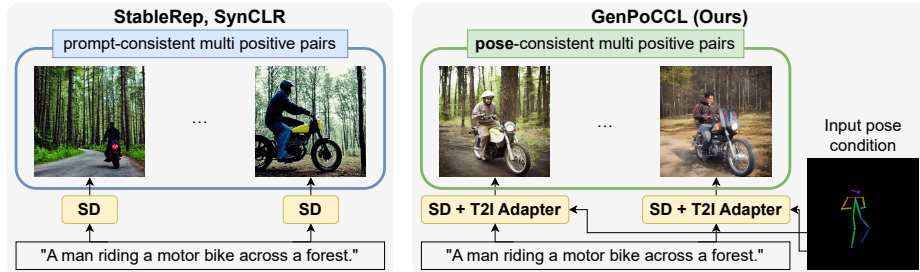


Fig. 1: We compare our method to StableRep [62] and SynCLR [61]. Both StableRep and SynCLR use a single prompt to generate semantically similar images which are then treated as positive pairs for contrastive learning. On the other hand, our GenPoCCL takes a step further by generating similar images from a same prompt and **same human body pose condition** for positive pairs for contrastive learning.

Meanwhile, image generation technology has advanced swiftly in recent years, achieving a quality that humans can hardly differentiate from actual images [21]. Alongside this trend, recent studies [30, 61, 62] have explored the pre-training of using generated images, and it has been reported that they achieve comparable or even superior performance to models pre-trained with real images. Thus, while pre-training with generated images indicates potential benefits, its effectiveness for tasks other than image classification and linear probing, particularly in practical scenarios, has not been confirmed. In addition to the rapid advancement in the quality of generated images, its controllability has also improved. Some researches [41, 48, 66] demonstrate the ability to control generated images in various methods, including line drawings, depth images, and human pose labels. Recent pre-training methods using generated images exploit the ability to generate consistent images from prompts, but the potential for consistent image generation with conditions other than prompts remains unexplored.

In this paper, we tackle the challenge of suboptimal performance in human-centric perception tasks, a common shortfall of pre-training methods using generated images, by proposing a novel method named GenPoCCL. The acronym GenPoCCL represents **Generated image leveraged Pose Consistent Contrastive Learning**. In GenPoCCL, we take advantage of the ability to generate images with uniform poses yet diverse appearances. By treating images generated from the same human body pose condition as positive pairs as shown in Fig. 1, we propose pose-consistent multi-positive contrastive learning to guide the model with human body pose constraints. We additionally introduce a special token named [POSE] token which allows to learn both discriminative human features and human-pose related features. Through GenPoCCL, images of the same pose can be mapped to proximate locations in the feature space, acquiring robust feature representations independent of background or human appearance. Consequently, this enables easier learning across human-centric perception tasks.

Remarkably, it achieves superior performance to current methods with under 1% of the generative data previously needed.

The contributions of this research are as follows:

- We propose generation of visually distinct images with identical human poses for self-supervised pre-training.
- We introduce GenPoCCL, a novel multi-positive contrastive learning approach that utilizes the generated pose-consistent appearance-varying images. It allows the model to learn structural features of the human body.
- We also introduce [POSE] token in GenPoCCL, which allows to learn both discriminative human features and human-pose related features.
- We experimentally show that GenPoCCL surpasses existing methods in a variety of human-centric perception tasks, with using only less than 1% amount of data compared to existing methods.

2 Related works

2.1 Image generation

Data has been always an important part of training a neural network. Depending on the task, a massive amount of data is needed in which obtaining them would become a tremendous task. On the other hand, generative models such as Normalizing Flow [22, 23, 39, 52], Generative Adversarial Network (GAN) [4, 28, 40], and especially diffusion models [34, 53, 56–59], have been showing a massive leap in generation quality, pushing learning with generated data to become the norm [2, 14, 33, 50, 54]. In recent years, diffusion models have gained popularity through their novel noise-denoising approach to generate highly detailed and realistic images. In addition, it has also been proven that diffusion model consistently beats other generative models in terms of generation quality [21]. Considering the importance of image quality in our work, we decide to opt for the diffusion model.

Diffusion models also offer flexibility in generation as they can be conditioned on various modalities. To generate a specific image, the most common way to guide the generation process is to use text as a guidance. Unfortunately, text-only guidance cannot capture the full preference on how the generated image should look like. To overcome this challenge, recent studies grant enhanced controllability in generation process by injecting extra features as guidance extracted from an external control module [41, 48, 66]. For example, T2I-adapter [48] and ControlNet [66] make it possible to generate image of human in specific pose by giving an OpenPose [6] bone image as input condition. Additionally, GLIGEN [41] allows the direct utilization of keypoint coordinates as input condition. Greater precision in controlling the image generation means more complex and better synthetic data can be obtained.

In this paper, we take advantage of controllable image generation to generate synthetic data consisting of pose-consistent, appearance-varying individuals. We then show how to effectively use them to train a neural network for representation learning task.

2.2 Representation learning

Representation learning is a learning methodology that allows a network to automatically discover meaningful representation based on the structure and relation of the provided training data. It focuses on identifying patterns and features that are important for understanding the data in a self-supervised manner. In recent years, masked image modeling (MIM) and contrastive learning (CL) emerged as the mainstream representation learning approach. MIM [3, 11, 31, 32, 49, 63] is a generative approach that learns representations by reconstructing the high portion of corrupted part in the given input based on the remaining information. On the other hand, CL [7, 12, 13, 29] is an approach which learns representations by discriminating between the similarity (dissimilarity) of positive (negative) image pairs via contrastive loss. Hence, having good positive and negative image pairs is very important for CL. Given a single original image, applying strong augmentations such as crop, resize, and color jitter, has been the standard to create multiple positive pairs [9]. However, recent studies show that creating positive pairs from different-yet-semantically-close data leads to better representation learning [25, 51, 62].

Recently, StableRep [62] has shown that Stable Diffusion [53] can be used to generate infinite variations of images to be treated as positive image pairs for CL. SynCLR [61] also proposes a pre-training method with a large-scale exclusively synthetic dataset constructed by generating images from LLM-created prompts. Similar to StableRep, they generate multiple semantically similar but visually diverse images from a single prompt, serving as multi-positive pairs for CL. SynthCLIP [30] also constructs a fully synthetic, large-scale text-image pairs dataset to train CLIP [51] model. Unfortunately, even though they show promising results, the effectiveness beyond classification and linear probing is still unconfirmed. Broader application of utilizing synthetic data for representation learning that target real life cases is yet to be explored.

Given its significance in numerous real-world scenarios, addressing human-centric understanding has emerged as a crucial challenge. While ImageNet [18] pre-training has been the standard, recent studies show that self-supervised pre-training approaches using a collection of human images yields improved understanding of human-centric attributes by the network [8, 16, 37, 60, 64]. Among these studies, HAP [64] shows promising results by proposing to incorporate human-part prior to guide masking strategy during MIM-based representation learning. In short, they select human body parts at random and mask the image patches that correspond to these selected areas. In addition, CL-equivalent structure-invariant alignment loss is also proposed to improve the network ability to capture the characteristic of human body.

Motivated by HAP success, we are encouraged to further improve it by utilizing synthetic data for the pre-training task. In our work, we exploit fine-grained controllable generation to generate specifically crafted images by fixing specific parts of the generated images, *e.g.*, varying human appearance with fixed pose. We then show how our proposed multi-positive CL is able to efficiently utilize the

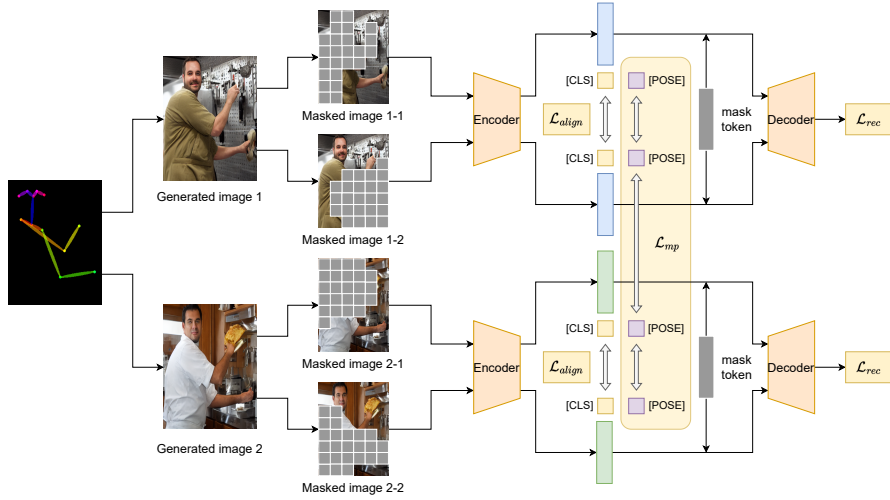


Fig. 2: Overall pipeline of our method. Utilizing Stable Diffusion [53] and T2I-Adapter [48], we generate pose-consistent images with varying appearances for contrastive learning from a single prompt and pose condition by altering the initial seed. In pre-training, selected human-part patches are masked following HAP [64]. We reconstruct images using a shared encoder-decoder, applying reconstruction loss \mathcal{L}_{rec} . Alignment of [CLS] tokens is achieved with HAP’s alignment loss \mathcal{L}_{align} , and we introduce a [POSE] token with a multi-positive contrastive loss \mathcal{L}_{mp} to refine pose and appearance learning.

specifically crafted generated image pairs to enhance the network understanding of better representations.

3 Proposed method

In our research, we employed generative models to generate images consistent with human body pose conditions, which are then utilized in self-supervised pre-training. Our training pipeline, detailed in Fig. 2, begins by generating multiple images from a single human pose label, as elaborated in Sec. 3.1. Subsequent steps include applying different masks in conjunction with the human body pose labels and processing these through a weight-shared encoder to extract features. We employ a [CLS] token for aligning features of the same identity using an alignment loss \mathcal{L}_{align} proposed in HAP [64], and introduce a [POSE] token to align features of people with consistent poses using a multi-positive contrastive learning objective \mathcal{L}_{mp} , which is further described in Sec. 3.2.

A simple alternative approach is to utilize input conditions and corresponding generated images as direct paired training data for downstream tasks. However, given the current performance of controllable generation models, generating a perfectly consistent image with the input condition remains a challenge, making them inadequate for supervised learning in downstream tasks that demand exact



Fig. 3: Examples of generated images with input human body pose condition. By varying the initial noise, we succeed in generating pose-consistent, appearance-varied images. We crop the images along with bounding-box labels.

labels. On the other hand, as mentioned in Sec. 2.2, HAP shows that indirect utilization of human body pose labels leads to better understanding of structural features of the human body. For this application, the current performance of controllable generation models is sufficient. Therefore, we leverage generated data as training data for self-supervised pre-training. Further details will be discussed in Sec. 4.2.

3.1 Pose-conditioned image generation

Motivated by the recent advancement in controllable image generation, we utilized the T2I-Adapter [48] for the image generation model. T2I-Adapter adds a small network to a pre-trained diffusion model, enabling image generation under various conditions. Leveraging a publicly available controllable model with human body poses, we generated five distinct images for a single human pose since MSCOCO dataset [42] has five slightly different caption labels for each image. Inputs for image generation were human body pose and caption labels derived from the MSCOCO dataset’s training split. Despite identical human body pose inputs, the use of varied initial noise generates images with appearance variations for each pose as shown in Fig. 3. The generated images are then cropped based on MSCOCO’s bounding box label to extract human area. Notably, MSCOCO’s labels for small human poses presented challenges, as the T2I-Adapter struggled to generate accurate representations. Consequently, bounding boxes smaller than 4,096 pixels were excluded. Furthermore, some MSCOCO labels correspond to incomplete human figures, which also prevented accurate human generation by the T2I-Adapter. Thus, images displaying fewer than five of the seventeen whole

body keypoints were likewise omitted. The refined dataset consists of 117,126 unique human poses with five variations each were utilized for pre-training. In this paper, we refer to this generated dataset as GenCOCO dataset.

To investigate the impact of increased data scale, we also created a large-scale generated dataset based on the LUPerson [26] dataset. We resized the human body pose pseudo-labels of images from the LUPerson dataset to 192 pixels in width, serving as input for image generation. Due to the absence of caption labels in the LUPerson dataset, a rule-based method was employed for caption generation, which was then used as input for image generation. This rule-based method is detailed in the supplementary material. As the data predominantly consists of full-body images, we do not perform any filtering. Consequently, 4,180,243 unique human poses with three variations each were utilized for pre-training. In this paper, we refer to this generated dataset as GenLUPerson dataset.

3.2 Pose-consistent multi-positive contrastive learning

HAP [64] suggests that implicitly learning structural features of the human body improves performance in human-centric perception tasks. Our proposed GenPoCCL applies multi-positive contrastive learning to bring features of images from the same pose closer together as shown in Fig. 2, enhancing the understanding of structural human body features. This property is unique to controllable generative models that can generate visually distinct images with identical human poses, where obtaining such real image pairs is deemed to be impossible. By adopting this learning approach, we make the feature extractor learn to project images with identical poses into around the same area in the feature space, acquiring robust features that are not influenced by the background or appearance. Consequently, this enables easier learning across human-centric perception tasks. To better capture structural human body features, we enhance the HAP pipeline with two key elements: a [POSE] token and a multi-positive contrastive loss.

Pose token. HAP employs a structure-invariant alignment loss to align the [CLS] token across two variations of masked images. Inspired by this, we considered employing a [CLS] token for multi-positive contrastive learning. However, we found that letting the [CLS] token both learn discriminative human features and to seek feature alignment across different image sharing the same pose is not optimal. Therefore, we proposed a new [POSE] token which tackles this problem. By incorporating the [POSE] token, we maintain the benefits of learning discriminative human characteristics via structure-invariant alignment loss and further strengthen the acquisition of the structural human body features. In practice, we demonstrate improved learning progression and enhanced performance in human-centric perception tasks, as shown in Sec. 4.3.

Multi-positive contrastive loss. Similar to StableRep [62], we describe multi-positive contrastive learning as a matching problem. Suppose that there is an

Algorithm 1: PyTorch-style pseudocode for our training pipeline

```

# enc: encoder
# dec: decoder
# tau: temperature
# minibatch x: [n, m, 3, h, w]
# keypoints kpts: [n, m, 17, 2]
# n poses, m images per pose
for x, kpts in loader:
    # apply different appearance augmentation for each (n*m) images
    x = appearance_augment(x)
    # apply same geometric augmentation for same pose images
    x = geometric_augment(x)
    x = cat(unbind(x, dim=1)) # [n*m, 3, h, w]
    # use keypoint labels to apply masks based on human body pose
    mask1 = gen_mask(cat(unbind(kpts, dim=1)))
    mask2 = gen_mask(cat(unbind(kpts, dim=1)))
    x1 = x * mask1 # add mask to input image
    h1 = enc(x1)
    cls1 = h1[:, 0, :] # extract [CLS] token
    cls1 = normalize(cls1)
    pose1 = h1[:, 1, :] # extract [POSE] token
    pose1 = normalize(pose1)
    mask_token1 = Parameter((n*m, d)) # d: embed dimension of decoder
    rec1 = dec(h1, mask_token1)
    x2 = x * mask2 # add another mask to input image
    h2 = enc(x2)
    cls2 = h2[:, 0, :] # extract [CLS] token
    cls2 = normalize(cls2)
    pose2 = h2[:, 1, :] # extract [POSE] token
    pose2 = normalize(pose2)
    mask_token2 = Parameter((n*m, d))
    rec2 = dec(h2, mask_token2)
    # compute loss only for masked region
    loss_rec = 0.5 * (MSE(rec1, x, mask1) + MSE(rec2, x, mask2))
    loss_align = 0.5 * (InfoNCE(cls1, cls2) + InfoNCE(cls2, cls1))
    loss_mp = 0.5 * (MPCLoss(pose1, pose2) + MPCLoss(pose2, pose1))
    loss = loss_rec +  $\gamma_1$  * loss_align +  $\gamma_2$  * loss_mp
    loss.backward()

```

encoded anchor sample \mathbf{a} and a collection of encoded candidates $\{\mathbf{b}_1, \mathbf{b}_2, \dots, \mathbf{b}_K\}$. We calculate a contrastive categorical distribution \mathbf{q} that indicates the likelihood of \mathbf{a} matching each of \mathbf{b} :

$$\mathbf{q}_i = \frac{\exp(\mathbf{a} \cdot \mathbf{b}_i / \tau)}{\sum_{j=1}^K \exp(\mathbf{a} \cdot \mathbf{b}_j / \tau)} \quad (1)$$

where τ represents a temperature hyper-parameter set to 0.2. Here, \mathbf{a} and all \mathbf{b} are l_2 normalized. Fundamentally, it can be viewed as a K -way softmax classification distribution over all encoded candidates. We can then interpret the ground-truth categorical distribution of \mathbf{p} as:

$$\mathbf{p}_i = \frac{\mathbb{1}_{\text{match}(\mathbf{a}, \mathbf{b}_i)}}{\sum_{j=1}^K \mathbb{1}_{\text{match}(\mathbf{a}, \mathbf{b}_j)}} \quad (2)$$

where the indicator function $\mathbb{1}_{\text{match}(\cdot, \cdot)}$ denotes whether the anchor and candidate match each other. Finally, the multi-positive contrastive loss can be calculated as the cross-entropy between the ground-truth distribution \mathbf{p} and the contrastive

distribution \mathbf{q} , which can be expressed as:

$$\mathcal{L}_{mp} = H(\mathbf{p}, \mathbf{q}) = - \sum_{i=1}^K \mathbf{p}_i \log \mathbf{q}_i \quad (3)$$

This loss function is closely related to that used in StableRep, yet it differs by aligning features between images from the same human pose rather than the same prompt. The Pytorch-like pseudocode of the batched multi-positive contrastive learning algorithm is described in the supplementary material.

3.3 Overall training pipeline

The overall loss function can be expressed as:

$$\mathcal{L} = \mathcal{L}_{rec} + \gamma_1 \mathcal{L}_{align} + \gamma_2 \mathcal{L}_{mp} \quad (4)$$

where \mathcal{L}_{rec} is the MSE loss for image reconstruction following [31], and \mathcal{L}_{align} is the InfoNCE loss for aligning features under varying masks following [64]. We use \mathcal{L}_{align} and \mathcal{L}_{mp} to align [CLS] and [POSE] tokens respectively. γ_1 and γ_2 are the weights to balance the three loss functions. We set γ_1 to 0.05 following [64], and also, γ_2 to 0.05 by default. The Pytorch-like pseudocode of our overall training pipeline is described in Algorithm 1. Each batch consists of $n \times m$ images, meaning that we sample m images for each of the n poses. Here we apply data augmentation; appearance augmentations vary across all images, while geometric augmentations remain consistent for images derived from the same pose. This ensures that geometric augmentations do not alter the consistency of human poses across images from the same pose.

4 Experiments

4.1 Settings

Pre-training. In our approach, as detailed in Sec. 3.1, the GenCOCO dataset and the GenLUPerson dataset are utilized for pre-training. Keypoint labels for both datasets are derived from the input human pose conditions used during image generation. The encoder model structure is based on the ViT-Base [24]. For the GenCOCO dataset, we use an input resolution of 256×192 and a batch size of 2,560 (*i.e.*, 64 poses \times 5 variations \times 8 GPUs). Similarly, for the GenLUPerson dataset, we maintain the same resolution and set the batch size to 6,144 (*i.e.*, 256 poses \times 3 variations \times 8 GPUs). Due to GPU memory limitations, we could not load all mini-batches at once and thus resorted to gradient accumulation. We adopt AdamW [45] as the optimizer in which the weight decay is set to 0.05. We use cosine decay learning rate scheduling [44] with the base learning rate set to $2.4e-3$. For experiments on the GenCOCO dataset, we set warmup epochs to 40 and total epochs to 800. For the GenLUPerson dataset, we set warmup epochs to 1 and total epochs to 40. The model parameters are initialized based on the

Xavier initialization method [27]. As mentioned in Sec. 3.3, appearance augmentations vary across all images, while geometric augmentations remain consistent for images derived from the same pose. Compared to the common settings in prior research [31, 64], we apply stronger augmentation to bridge the domain gap between real and generated images. We additionally adopt various types of augmentations such as random rotation, random blur, *etc.* We empirically validate the effectiveness of stronger augmentation in Sec. 4.3. Details of specific augmentations are provided in the supplementary material. After pre-training, the encoder is retained along with task-specific heads to address the downstream human-centric perception tasks, while other modules are discarded.

Human-centric perception tasks. We perform quantitative evaluation on six benchmarks over four human-centric perception tasks. These tasks include 2D human pose estimation on MPII [1] and MSCOCO [42], person ReID on Market-1501 [67], text-to-image person ReID on RSTPReid [68], and pedestrian attribute recognition on PA-100K [43] and PETA [19]. For 2D pose estimation, we employ PCKh and AP as metrics for MPII and MSCOCO respectively. Our framework is built upon the MMPose codebase [17]. In person ReID, we adopt the method of Lu *et al.* [46] and report mAP. For text-to-image person ReID, we report Rank-1 using the approach of Shao *et al.* [55]. In pedestrian attribute recognition, we report mean accuracy (mA) with the strategy proposed by Jia *et al.* [38]. Further training specifics are available in the supplementary material.

4.2 Main results

In this section, we benchmark human-centric perception tasks to contrast the efficacy of models pre-trained with conventional methods using generated images, against those trained with our GenPoCCL. Notably, GenPoCCL_{COCO} requires only ~ 0.6 M generated samples, less than 1% of the data volume used by StableRep (Tab. 1a). Even with this smaller dataset, GenPoCCL succeeds in capturing structural features of the human body, outperforming StableRep in subsequent human-centric perception tasks. Also, as shown in Tab. 1, increasing the scale of the dataset has the potential to further improve performance. While some tasks do not show improved performance, the reasons are discussed in detail in Sec. 4.5. Please note that although the performance of HAP trained only with real images surpasses GenPoCCL, our goal is to utilize generated data for pre-training. Hence, the following section details a performance comparison between GenPoCCL trained on the GenCOCO dataset and StableRep trained on the GenCC12M dataset, focusing on evaluations across various tasks.

2D pose estimation. The goal of this task is to localize human pose keypoints displayed in the image. Tab. 1b shows that GenPoCCL outperforms StableRep by +0.9% on MPII [1], +0.1% on MSCOCO [42], respectively. Also, compared to an alternative approach which directly utilizes input conditions and corresponding generated images as direct paired training data, GenPoCCL outperforms

Table 1: Main results. We compare GenPoCCL with representative pre-training methods. *Syn.* means utilization of synthetic data during pre-training. [†] indicates the results of our replication experiments using the pre-trained model and the implementation published by [64]. We report mean performance over three independent trials.

(a) **Dataset information.** We compare the number of training data for each competing method.

Method	Datasets	Samples
HAP [64]	LUPerson	2.1M
StableRep _{CC} [62]	GenCC12M	83M
StableRep _{Red} [62]	GenRedCaps	105M
SynCLR [61]	SynCaps-150M	600M
SynthCLIP [30]	SynthCI-30M	30M
GenPoCCL _{COCO}	GenCOCO	0.59M
GenPoCCL _{LU}	GenLUPerson	12M

(c) **Person re-id.** We evaluate on Market-1501 dataset [67]. mAP(%) is reported.

Method	Syn.	Market-1501
HAP [64]	X	91.7
HAP [†] [64]	X	92.0
StableRep _{CC} [62]	✓	70.5
StableRep _{Red} [62]	✓	77.5
SynCLR [61]	✓	86.6
SynthCLIP [30]	✓	81.5
GenPoCCL _{COCO}	✓	83.0
GenPoCCL _{LU}	✓	86.7

(b) **2D pose estimation.** PCKh(%) is reported for MPII and AP(%) is reported for MSCOCO.

Method	Syn.	MSCOCO	MPII
HAP [64]	X	75.9	91.8
HAP [†] [64]	X	75.8	91.2
StableRep _{CC} [62]	✓	73.9	88.3
StableRep _{Red} [62]	✓	74.0	88.0
SynCLR [61]	✓	74.3	88.0
SynthCLIP [30]	✓	73.1	86.0
Supervised	✓	71.3	-
GenPoCCL _{COCO}	✓	74.1	89.2
GenPoCCL _{LU}	✓	74.2	89.7

(d) **Text-to-image person re-id.** We evaluate on RSTPReid dataset [68]. Rank-1(%) is reported.

Method	Syn.	RSTPReid
HAP [64]	X	49.4
HAP [†] [64]	X	54.4
StableRep _{CC} [62]	✓	43.0
StableRep _{Red} [62]	✓	42.8
SynCLR [61]	✓	21.8
SynthCLIP [30]	✓	21.7
GenPoCCL _{COCO}	✓	46.2
GenPoCCL _{LU}	✓	45.2

(e) **Attribute recognition.** We evaluate on PA-100K [43] and PETA [19] datasets. mA(%) is reported.

Method	Syn.	PA-100K	PETA
HAP [64]	X	86.5	88.4
HAP [†] [64]	X	81.8	87.9
StableRep _{CC} [62]	✓	78.4	85.2
StableRep _{Red} [62]	✓	77.4	84.5
SynCLR [61]	✓	63.4	72.7
SynthCLIP [30]	✓	60.6	72.5
GenPoCCL _{COCO}	✓	79.0	85.0
GenPoCCL _{LU}	✓	77.8	83.6

Table 2: Ablation analysis. *PoCCL*, and *[POSE]* stand for pose-consistent multi-positive contrastive learning and *[POSE]* token, respectively.

method	PoCCL	[POSE]	MPII	Market-1501	RSTPReid	PA-100K
baseline-HAP			88.7	81.6	41.4	78.5
GenPoCCL-0	✓		89.0	83.2	39.4	78.4
GenPoCCL	✓	✓	89.2	83.0	46.2	79.0

+2.8% on MSCOCO dataset. This result indicates that the consistency between input conditions and corresponding generated images is insufficient for direct supervision, yet adequate for indirect supervision.

Person ReID. The purpose of this task is to retrieve a person of interest across multiple non-overlapping cameras. Tab. 1c shows that GenPoCCL outperforms StableRep by +5.5% on Market-1501 [67] dataset. Interestingly, the gradient explodes for the StableRep pre-trained model in very early training iterations, so we clamp the training loss to stabilize training.

Text-to-image person ReID. The goal of this task is to search for pedestrian images of a specific identity via textual descriptions. Tab. 1d shows that GenPoCCL outperforms StableRep by +3.2% on RSTPReid [68] dataset.

Pedestrian attribute recognition. The aim of this task is to assign multiple attributes to one pedestrian image. Tab. 1e shows that GenPoCCL outperforms StableRep by +0.6% on PA100K [43] dataset, and achieves comparable performance on PETA [19] dataset. We argue that since human body pose understanding is less important than appearance understanding in this task, GenPoCCL does not show remarkable performance.

4.3 Ablation study

Ablation studies for the proposed components are detailed in Tab. 2. The baseline is denoted as Baseline-HAP, which employed HAP’s default settings on the GenCOCO dataset.

To demonstrate the efficacy of the proposed pose-consistent multi-positive contrastive learning, we trained a model by solely adding it to the baseline-HAP, which we refer to as GenPoCCL-0. In other words, GenPoCCL-0 employs a [CLS] token to learn both HAP’s structure-invariant alignment and our proposed pose-consistent multi-positive contrastive loss. Compared with baseline-HAP and GenPoCCL-0, our proposed GenPoCCL results in +0.3% on MPII, and +1.6% on Market-1501. Unfortunately, the performance on RSTPReid decreased by 2.0%. These results show that letting the [CLS] token both learn

Table 3: Performance comparison of our proposed GenPoCCL with different data augmentation settings. We additionally adopt several types of augmentations (*e.g.*, random rotation, random blur, *etc.*) for stronger augmentation. We show that strong augmentation is beneficial to capture important representation during pre-training.

Augmentation	MPII	Market-1501	RSTPReid	PA-100K
match [31,64]	87.7	75.8	42.0	76.5
stronger	89.2	83.0	46.2	79.0

discriminative human features and to seek feature alignment across different image sharing the same pose is suboptimal, as discussed in Sec. 3.2. We will show in the following paragraph incorporating the [POSE] token is highly effective for addressing this problem.

Compared with GenPoCCL-0 and GenPoCCL, which incorporating [POSE] token, results in +6.8% on RSTPReid, and +0.6% on PA-100K. On the other hand, the performance on Market-1501 decreased by 0.2%. In text-to-image ReID (RSTPReid), focusing on more detailed human features is necessary. Our proposed [POSE] token allows for the extraction of both discriminative human features and human-pose related features, which is critical for this task.

As mentioned in Sec. 4.1, we adopt stronger data augmentation than the common settings in prior research [31,64]. As shown in Tab. 3, our proposed stronger data augmentation results in +7.2% on Market-1501, and +4.2 % on RSTPReid. We consider this is because stronger data augmentation bridges the domain gap between real and generated images.

Overall, by integrating pose-consistent multi-positive contrastive learning and the addition of the [POSE] token, our GenPoCCL outperforms the baseline-HAP. Consequently, our proposed GenPoCCL outperformed StableRep in various human-centric perception tasks even with a smaller dataset, demonstrating significant benefits of the design of our GenPoCCL.

4.4 Qualitative results

We visualize intermediate features of the pre-trained feature extractor by utilizing t-SNE [47]. Initially, for each of the six human pose pseudo-labels from the LUPerson dataset, we generate 64 images with consistent poses and varied appearances. Subsequently, we extract and visualize their features using pre-trained models. As shown in Fig. 4, compared to the StableRep pre-trained model, our GenPoCCL pre-trained model is able to map images with similar poses to proximate spaces. As indicated by the red circles, the StableRep pre-trained model struggles to discriminate between poses with one hand raised and those with both hands raised, whereas our model succeeds in distinguishing between them. It means our GenPoCCL pre-trained model succeeded in learning the structural features of the human body. Consequently, our GenPoCCL pre-trained model easily adapts to various human-centric perception tasks, resulting in better performance.

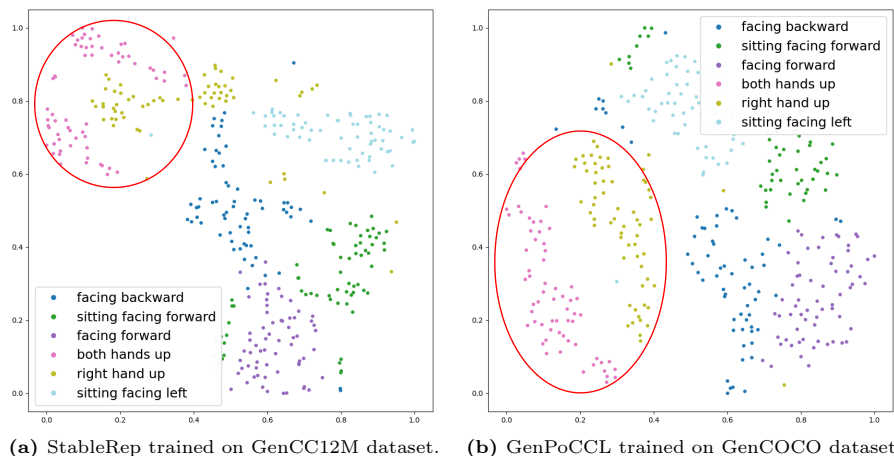


Fig. 4: Comparison of t-SNE visualization between StableRep and GenPoCCL. As we can see, GenPoCCL is able to cleanly separate the features of different poses. It implies that GenPoCCL better captures human pose representation.

4.5 Limitations

While our method is proven to be effective, we recognize its limitations. Firstly, the quality of the generated images can be suboptimal, particularly in the case of human faces. Additionally, we do not specifically evaluate the quality of pose consistency between the generated image and the input condition. We consider these to be one of the reasons for the performance degradation compared to methods using real data. Furthermore, inconsistencies between generated images and provided captions or conditions may compromise the generated data’s quality and utility. Additionally, our GenLUPerson dataset is created using a rule-based caption generation scheme, which is considered to be less than optimal. We consider that employing large language models (LLMs) for caption generation, akin to the SynCLR [61] or SynthCLIP [30] approach, might enhance the quality and diversity of the synthetic captions.

5 Conclusion

This paper presents the first investigation into pre-training solely with generated images for human-centric perception tasks and introduces a novel method named GenPoCCL. By generating pose-consistent, appearance-varying images and employing pose-consistent multi-positive contrastive learning to align their features, we experimentally demonstrated the ability to effectively capture the structural features of the human body, even with synthetic images. Even with merely less than 1% of the data volume used by StableRep, GenPoCCL outperforms StableRep across various human-centric perception tasks.

Supplementary Materials for Multi Positive Contrastive Learning with Pose-Consistent Generated Images

A Details of multi-positive contrastive learning

The Pytorch-like pseudocode of the batched pose-consistent multi-positive contrastive learning algorithm is described in Algorithm 2. We first assign consistent labels to images generated from the same human pose input. We then utilize cross-entropy loss during training to encourage the model to align the features corresponding to identical poses and distinctly separate the features from different ones.

Algorithm 2: PyTorch-style pseudocode for multi-positive contrastive loss

```
# latent vector z1: [n*m, 1]
# latent vector z2: [n*m, 1]
# n poses, m images per pose
def MPCLoss(z1, z2)
    # compute ground-truth distribution p
    label = range(n)
    # label images from same pose consistently by repeating m times
    label = label[:, None].repeat(1, m).flatten()
    p = (label.view(-1, 1) == label.view(1, -1))
    p.fill_diagonal(0) # self masking
    p /= p.sum(1)

    # compute contrastive distribution q
    logits = einsum(z1, z2) / tau
    logits.fill_diagonal(-1e9) # self masking
    q = softmax(logits, dim=1)

    H(p, q).backward()

def H(p, q): # cross-entropy
    return - (p * log(q)).sum(1).mean()
```

B Details of strong data augmentation

As introduced in the main paper, we adopt stronger data augmentation settings than existing methods [31, 64] for bridging domain gaps between real images and generated images. We list detailed settings of data augmentation in Tab. A.

Table A: Details of data augmentation used in pre-training. We use specific functions from Albumentations [5] package mentioned in *augmentation* column. In addition, their parameters are listed in a *parameters* column.

augmentation	match [31, 64]	stronger	parameters	probability
ColorJitter	✗	✓	brightness=0.2 contrast=0.2 saturation=0.2 hue=0.2	0.8
GaussianBlur	✗	✓	blur_limit=(3,7) sigma_limit=0	0.8
ToGray	✗	✓	-	0.2
Solarize	✗	✓	threshold=128	0.2
HorizontalFlip	✓	✓	-	0.5
ShiftScaleRotate	✗	✓	shift_limit=0.0 scale_limit=0.0 rotate_limit=45 interpolation=2♣ border_mode=0♦ value=pix_mean♣	1.0
RandomResizedCrop	✓	✓	height=256 width=192 scale=(0.8,1.0) ratio=(3/8, 2/3) interpolation=2	1.0

♣ cv2.INTER_CUBIC=2.

♦ cv2.BORDER_CONSTANT=0.

♣ The mean pixel value used for input normalization.

In our settings, pix_mean=(123.675, 116.28, 103.53).

C Hyperparameters of human-centric perception tasks

C.1 2D human pose estimation

We evaluate the proposed GenPoCCL for 2D human pose estimation on MPII [1] and MSCOCO [42] datasets. Leveraging the MMPose codebase [17], we incorporate ViTPose [65] following HAP [64]. The input resolution is fixed at 256×192

pixels. Data augmentations are random horizontal flipping, half body transformations, and random scaling and rotation, which are same settings as HAP. We use mean square error(MSE) as the loss function to minimize the difference between predicted and ground-truth heatmaps. Please refer to Tab. B for the hyper-parameter specifications.

Table B: Hyper-parameters of 2D human pose estimation.

dataset	batch size	epochs	learning rate	optimizer	weight decay	layer decay	drop path
MPII	512	210	2.0e-4	Adam	-	-	0.30
MSCOCO	512	210	5.0e-4	AdamW	0.1	0.80	0.30

C.2 Person ReID

We evaluate the proposed GenPoCCL for person ReID on Market-1501 [67] dataset. We leverage the codebase of HAP, which originates from MALE [46]. The input resolution is fixed at 256×128 pixels. Data augmentations are resizing, random flipping, padding, and random cropping, which are same settings as HAP. We use a cross-entropy loss and a triplet loss with equal weights of 0.5. Please refer to Tab. C for the hyper-parameter specifications.

Table C: Hyper-parameters of person ReID.

dataset	batch size	epochs	learning rate	optimizer	weight decay	layer decay	drop path
Market-1501	64	100	8.0e-3	AdamW	0.05	0.40	0.10

C.3 Text-to-image person ReID

We evaluate the proposed GenPoCCL for text-to-image person ReID on RST-PReid [68] dataset. We leverage the codebase of HAP, which originates from LGUR [55]. The input resolution is fixed at 384×128 pixels. Data augmentations are resizing and random horizontal flipping, which are same settings as HAP. BERT [20] is utilized to extract text embeddings, which are then fed into bidirectional LSTM (Bi-LSTM) [35]. Feature dimensions of image and text embeddings are both fixed at 384. The BERT is frozen while Bi-LSTM and ViT are trained with a cross-entropy loss and a ranking loss. Please refer to Tab. D for the hyper-parameter specifications.

Table D: Hyper-parameters of text-to-image person ReID.

dataset	batch size	epochs	learning rate	optimizer
RSTPReid	64	60	1.0e-3	Adam

C.4 Pedestrian attribute recognition

We evaluate the proposed GenPoCCL for pedestrian attribute recognition on PA-100K [43] and PETA [19] dataset. We leverage the codebase of HAP, which originates from Rethinking of PAR [38]. The input resolution is fixed at 256×192 pixels. Data augmentations are resizing and random horizontal flipping, which are same settings as HAP. The binary cross-entropy loss is utilized for multi-class classification training. Please refer to Tab. E for the hyper-parameter specifications.

Table E: Hyper-parameters of pedestrian attribute recognition.

dataset	batch size	epochs	learning rate	optimizer	weight decay
PA-100K	64	55	1.7e-4	AdamW	5.0e-4
PETA	64	50	1.9e-4	AdamW	5.0e-4

D Caption generation method

As introduced in the main paper, we adopt rule-based method to generate captions for GenLUPerson dataset. Firstly, we prepare two types of formats of captions as shown in Tab. F. We choose one of them randomly based on the probability written in Tab. F. Then, we randomly sample expressions for each variable contained in the format. The candidates of each variable is shown in Tab. G. Through this approach, we can obtain captions such as "An Asian girl wearing sky blue one-piece" to be used as inputs for image generation.

Table F: Two types of rule-based formats used for generating captions. Each bracket represents a variable where the choices are detailed in Tab. G.

format	probability
(race) (identity) wearing (color1) (upper cloth) and (color2) (lower cloth)	0.7
(race) (identity) wearing (color1) (clothing)	0.3

Table G: Candidates of each variable. We try our best to ensure inclusivity across all races to enrich generational diversity for our work.

variables	choices
race	An Asian, An Australian, An African, An European, A North American, A South American
identity	man, woman, boy, girl
color1, color2	aurora, baby pink, begonia, bougainvillea, camellia, coral pink, dawn pink, flamingo, flesh pink, mallow, nail pink, old rose, pastel pink, peach pink, pink, rose pink, salmon pink, shell pink, shrimp pink, sunrise pink, alizarin red, azalea, burgundy, carmine, cherry red, crimson, garnet, lacquer red, magenta, poppy red, raspberry, red, rose red, ruby, scarlet, shrimp red, signal red, strawberry, turquoise red, wine red, apricot, brick red, brunt sienna, carrot, cinnamon, coral red, nasturtium, orange, persimmon orange, pumpkin, tangerine, tiger lily, topaz, vermilion, bister, bronze, brown, buff, burnt umber, camel, chestnut brown, chocolate, coffee brown, copper, cork, hazel brown, henna, khaki, mahogany brown, maroon, raw-sienna, sand beige, sepia, tan, terracotta, umber, bamboo, beige, blond, buttercup yellow, canary, chartreuse yellow, flesh, fragrant olive, gold, jasmine, jaune brillant, lemon yellow, lime green, maize, marigold, mimosa, mustard, Naples yellow, primrose yellow, saffron yellow, straw, sunflower, yellow ocher, yellow, apple green, aquamarine, avocado, billiard green, bottle green, celadon, chartreuse green, cobalt green, emerald, ever green, forest green, grass green, green, iron blue, ivy green, jade, jasper green, laurel green, leaf green, malachite green, marine blue, moss green, olive, parrot green, peppermint green, sage green, spruce, teal green, turquoise blue, turquoise green, viridian, aqua, baby blue, blue, candy blue, cerulean, cobalt blue, cyan, delft blue, duck blue, fog blue, forget me not, frosty blue, gentian blue, hyacinth, hydrangea blue, indigo, ink blue, lapislazuli, majolica blue, midnight blue, moonlight blue, navy blue, Nile blue, oriental blue, peacock blue, powder blue, Prussian blue, royal blue, saxe blue, sky blue, smalt, ultramarine, wedgewood blue, amaranth purple, bellflower, claret, crocus, eggplant, fuchsia, grape, heliotrope, iris, lavender, lilac, mauve, mulberry, orchid, pansy, pearl gray, peony, purple, raisin, royal purple, taupe, Victoria violet, violet, wistaria, black, charcoal gray, cloud gray, dusky gray, ebony, eggshell, gray, gunmetal gray, ivory black, ivory, lamp black, milky white, pearl white, slate gray, snow white, taupe, white
upper cloth	t-shirt, polo shirt, dress shirt, sweater, hoodie, tank top, crop top, blouse, cardigan, jacket, coat, vest, blazer, bolero, poncho, shawl, jersey, sweatshirt, pullover, henley shirt, rugby shirt, turtleneck, peplum top, halter top, tube top, camisole, corset, bustier
lower cloth	jeans, trousers, shorts, skirt, leggings, joggers, sweatpants, chinos, cargo pants, capris, culottes, harem pants, palazzo pants, pencil skirt, mini skirt, maxi skirt, A-line skirt, pleated skirt, wrap skirt, sarong, bermuda shorts, hot pants, board shorts, cycling shorts, bell-bottoms, slacks, tights, kilt
clothing	dress, overalls, jumpsuit, romper, playsuit, one-piece, dungarees, unitard, catsuit, salopettes, boiler suit, coveralls, flight suit, kimono, sari, cheongsam, hanbok, kaftan, toga, tunic

D.1 Discussions

In our study, we utilized captions specifying race to generate diverse images which reflect a variety of racial features, as they are employed in the dataset for training generative models. While we use terms referring to specific regions or

ethnicities, it is strictly for scientific analysis and advancement in image generation technology, without any intent to promote stereotypes or biases. The terms are carefully chosen to respect and accurately represent the diversity of each region and ethnicity. These expressions are essential within the research context and are indispensable for achieving our objectives. We commit to adhering to ethical standards in research and respecting the dignity and diversity of all individuals.

References

1. Andriluka, M., Pishchulin, L., Gehler, P., Schiele, B.: 2d human pose estimation: New benchmark and state of the art analysis. In: CVPR. pp. 3686–3693 (2014) [10](#), [16](#)
2. Azizi, S., Kornblith, S., Saharia, C., Norouzi, M., Fleet, D.J.: Synthetic data from diffusion models improves imagenet classification. arXiv preprint arXiv:2304.08466 (2023) [3](#)
3. Bao, H., Dong, L., Piao, S., Wei, F.: Beit: Bert pre-training of image transformers. arXiv preprint arXiv:2106.08254 (2021) [4](#)
4. Brock, A., Donahue, J., Simonyan, K.: Large scale gan training for high fidelity natural image synthesis. arXiv preprint arXiv:1809.11096 (2018) [3](#)
5. Buslaev, A., Iglovikov, V.I., Khvedchenya, E., Parinov, A., Druzhinin, M., Kalinin, A.A.: Albumentations: Fast and flexible image augmentations. *Information* **11**(2) (2020). <https://doi.org/10.3390/info11020125>, <https://www.mdpi.com/2078-2489/11/2/125> [16](#)
6. Cao, Z., Simon, T., Wei, S.E., Sheikh, Y.: Realtime multi-person 2d pose estimation using part affinity fields. In: CVPR. pp. 7291–7299 (2017) [3](#)
7. Caron, M., Touvron, H., Misra, I., Jégou, H., Mairal, J., Bojanowski, P., Joulin, A.: Emerging properties in self-supervised vision transformers. In: ICCV. pp. 9650–9660 (2021) [4](#)
8. Chen, C., Ye, M., Qi, M., Wu, J., Jiang, J., Lin, C.W.: Structure-aware positional transformer for visible-infrared person re-identification. *IEEE Transactions on Image Processing* **31**, 2352–2364 (2022) [4](#)
9. Chen, T., Kornblith, S., Norouzi, M., Hinton, G.: A simple framework for contrastive learning of visual representations. In: ICML (2020) [4](#)
10. Chen, W., Xu, X., Jia, J., Luo, H., Wang, Y., Wang, F., Jin, R., Sun, X.: Beyond appearance: a semantic controllable self-supervised learning framework for human-centric visual tasks. In: CVPR. pp. 15050–15061 (2023) [1](#)
11. Chen, X., Ding, M., Wang, X., Xin, Y., Mo, S., Wang, Y., Han, S., Luo, P., Zeng, G., Wang, J.: Context autoencoder for self-supervised representation learning. *IJCV* **132**(1), 208–223 (2024) [4](#)
12. Chen, X., Fan, H., Girshick, R., He, K.: Improved baselines with momentum contrastive learning. arXiv preprint arXiv:2003.04297 (2020) [4](#)
13. Chen, X., Xie, S., He, K.: An empirical study of training self-supervised vision transformers. In: ICCV (2021) [4](#)
14. Chen, Y., Li, W., Chen, X., Gool, L.V.: Learning semantic segmentation from synthetic data: A geometrically guided input-output adaptation approach. In: CVPR. pp. 1841–1850 (2019) [3](#)
15. Chen, Z., Li, Q., Wang, X., Yang, W.: Liftedcl: Lifting contrastive learning for human-centric perception. In: ICLR (2022) [1](#)

16. Ci, Y., Wang, Y., Chen, M., Tang, S., Bai, L., Zhu, F., Zhao, R., Yu, F., Qi, D., Ouyang, W.: Unihcp: A unified model for human-centric perceptions. In: CVPR. pp. 17840–17852 (2023) [1](#), [4](#)
17. Contributors, M.: Openmmlab pose estimation toolbox and benchmark. <https://github.com/open-mmlab/mmpose> (2020) [10](#), [16](#)
18. Deng, J., Dong, W., Socher, R., Li, L.J., Li, K., Fei-Fei, L.: Imagenet: A large-scale hierarchical image database. In: CVPR. pp. 248–255. Ieee (2009) [4](#)
19. Deng, Y., Luo, P., Loy, C.C., Tang, X.: Pedestrian attribute recognition at far distance. In: ACM MM. pp. 789–792 (2014) [10](#), [11](#), [12](#), [18](#)
20. Devlin, J., Chang, M.W., Lee, K., Toutanova, K.: Bert: Pre-training of deep bidirectional transformers for language understanding. arXiv preprint arXiv:1810.04805 (2018) [17](#)
21. Dhariwal, P., Nichol, A.: Diffusion models beat gans on image synthesis. NeurIPS **34**, 8780–8794 (2021) [2](#), [3](#)
22. Dinh, L., Krueger, D., Bengio, Y.: Nice: Non-linear independent components estimation. arXiv preprint arXiv:1410.8516 (2014) [3](#)
23. Dinh, L., Sohl-Dickstein, J., Bengio, S.: Density estimation using real nvp. arXiv preprint arXiv:1605.08803 (2016) [3](#)
24. Dosovitskiy, A., Beyer, L., Kolesnikov, A., Weissenborn, D., Zhai, X., Unterthiner, T., Dehghani, M., Minderer, M., Heigold, G., Gelly, S., Uszkoreit, J., Houlsby, N.: An image is worth 16x16 words: Transformers for image recognition at scale. In: ICLR (2021), <https://openreview.net/forum?id=YicbFdNTTy> [9](#)
25. El Banani, M., Desai, K., Johnson, J.: Learning visual representations via language-guided sampling. In: CVPR. pp. 19208–19220 (2023) [4](#)
26. Fu, D., Chen, D., Bao, J., Yang, H., Yuan, L., Zhang, L., Li, H., Chen, D.: Unsupervised pre-training for person re-identification. CVPR (2021) [7](#)
27. Glorot, X., Bengio, Y.: Understanding the difficulty of training deep feedforward neural networks. In: Teh, Y.W., Titterton, M. (eds.) Proceedings of the Thirteenth International Conference on Artificial Intelligence and Statistics. Proceedings of Machine Learning Research, vol. 9, pp. 249–256. PMLR (2010). <https://doi.org/10.1121/1.4767975>. [9](#) [10](#)
28. Goodfellow, I., Pouget-Abadie, J., Mirza, M., Xu, B., Warde-Farley, D., Ozair, S., Courville, A., Bengio, Y.: Generative adversarial networks. Communications of the ACM **63**(11), 139–144 (2020) [3](#)
29. Grill, J.B., Strub, F., Altché, F., Tallec, C., Richemond, P., Buchatskaya, E., Doherty, C., Avila Pires, B., Guo, Z., Gheshlaghi Azar, M., et al.: Bootstrap your own latent—a new approach to self-supervised learning. NeurIPS **33**, 21271–21284 (2020) [4](#)
30. Hammoud, H.A.A.K., Itani, H., Pizzati, F., Torr, P., Bibi, A., Ghanem, B.: Synthclip: Are we ready for a fully synthetic clip training? arXiv preprint arXiv:2402.01832 (2024) [1](#), [2](#), [4](#), [11](#), [14](#)
31. He, K., Chen, X., Xie, S., Li, Y., Dollár, P., Girshick, R.: Masked autoencoders are scalable vision learners. In: CVPR (2022) [4](#), [9](#), [10](#), [13](#), [16](#)
32. He, K., Fan, H., Wu, Y., Xie, S., Girshick, R.: Momentum contrast for unsupervised visual representation learning. In: CVPR. pp. 9729–9738 (2020) [4](#)
33. He, R., Sun, S., Yu, X., Xue, C., Zhang, W., Torr, P., Bai, S., Qi, X.: Is synthetic data from generative models ready for image recognition? arXiv preprint arXiv:2210.07574 (2022) [3](#)
34. Ho, J., Jain, A., Abbeel, P.: Denoising diffusion probabilistic models. NeurIPS **33**, 6840–6851 (2020) [3](#)

35. Hochreiter, S., Schmidhuber, J.: Long short-term memory. *Neural computation* **9**(8), 1735–1780 (1997) [17](#)
36. Hong, F., Pan, L., Cai, Z., Liu, Z.: Versatile multi-modal pre-training for human-centric perception. In: CVPR. pp. 16156–16166 (2022) [1](#)
37. Hong, F., Pan, L., Cai, Z., Liu, Z.: Versatile multi-modal pre-training for human-centric perception. In: CVPR. pp. 16156–16166 (2022) [4](#)
38. Jia, J., Huang, H., Chen, X., Huang, K.: Rethinking of pedestrian attribute recognition: A reliable evaluation under zero-shot pedestrian identity setting. *arXiv preprint arXiv:2107.03576* (2021) [10](#), [18](#)
39. Kingma, D.P., Dhariwal, P.: Glow: Generative flow with invertible 1x1 convolutions. *NeurIPS* **31** (2018) [3](#)
40. Ledig, C., Theis, L., Huszár, F., Caballero, J., Cunningham, A., Acosta, A., Aitken, A., Tejani, A., Totz, J., Wang, Z., et al.: Photo-realistic single image super-resolution using a generative adversarial network. In: CVPR. pp. 4681–4690 (2017) [3](#)
41. Li, Y., Liu, H., Wu, Q., Mu, F., Yang, J., Gao, J., Li, C., Lee, Y.J.: Gligen: Open-set grounded text-to-image generation. *CVPR* (2023) [2](#), [3](#)
42. Lin, T.Y., Maire, M., Belongie, S., Hays, J., Perona, P., Ramanan, D., Dollár, P., Zitnick, C.L.: Microsoft coco: Common objects in context. In: *ECCV*. pp. 740–755. Springer (2014) [6](#), [10](#), [16](#)
43. Liu, X., Zhao, H., Tian, M., Sheng, L., Shao, J., Yi, S., Yan, J., Wang, X.: Hydraplus-net: Attentive deep features for pedestrian analysis. In: *ICCV*. pp. 350–359 (2017) [10](#), [11](#), [12](#), [18](#)
44. Loshchilov, I., Hutter, F.: SGDR: Stochastic gradient descent with warm restarts. In: *ICLR* (2017), <https://openreview.net/forum?id=Skq89Scxx> [9](#)
45. Loshchilov, I., Hutter, F.: Decoupled weight decay regularization. In: *ICLR* (2019), <https://openreview.net/forum?id=Bkg6RiCqY7> [9](#)
46. Lu, Y., Zhang, M., Lin, Y., Ma, A.J., Xie, X., Lai, J.: Improving pre-trained masked autoencoder via locality enhancement for person re-identification. In: *Chinese Conference on Pattern Recognition and Computer Vision (PRCV)*. pp. 509–521. Springer (2022) [10](#), [17](#)
47. Van der Maaten, L., Hinton, G.: Visualizing data using t-sne. *Journal of machine learning research* **9**(11) (2008) [13](#)
48. Mou, C., Wang, X., Xie, L., Wu, Y., Zhang, J., Qi, Z., Shan, Y., Qie, X.: T2i-adapter: Learning adapters to dig out more controllable ability for text-to-image diffusion models. *arXiv preprint arXiv:2302.08453* (2023) [2](#), [3](#), [5](#), [6](#)
49. Peng, Z., Dong, L., Bao, H., Ye, Q., Wei, F.: Beit v2: Masked image modeling with vector-quantized visual tokenizers. *arXiv preprint arXiv:2208.06366* (2022) [4](#)
50. Pumarola, A., Sanchez-Riera, J., Choi, G., Sanfeliu, A., Moreno-Noguer, F.: 3dpeople: Modeling the geometry of dressed humans. In: *CVPR*. pp. 2242–2251 (2019) [3](#)
51. Radford, A., Kim, J.W., Hallacy, C., Ramesh, A., Goh, G., Agarwal, S., Sastry, G., Askell, A., Mishkin, P., Clark, J., et al.: Learning transferable visual models from natural language supervision. In: *ICML*. pp. 8748–8763. PMLR (2021) [4](#)
52. Rezende, D., Mohamed, S.: Variational inference with normalizing flows. In: *ICML*. pp. 1530–1538. PMLR (2015) [3](#)
53. Rombach, R., Blattmann, A., Lorenz, D., Esser, P., Ommer, B.: High-resolution image synthesis with latent diffusion models. In: *CVPR*. pp. 10684–10695 (2022) [3](#), [4](#), [5](#)

54. Sariyildiz, M.B., Alahari, K., Larlus, D., Kalantidis, Y.: Fake it till you make it: Learning transferable representations from synthetic imagenet clones. In: CVPR (2023) [3](#)
55. Shao, Z., Zhang, X., Fang, M., Lin, Z., Wang, J., Ding, C.: Learning granularity-unified representations for text-to-image person re-identification. In: ACM MM. pp. 5566–5574 (2022) [10](#), [17](#)
56. Song, J., Meng, C., Ermon, S.: Denoising diffusion implicit models. arXiv preprint arXiv:2010.02502 (2020) [3](#)
57. Song, Y., Ermon, S.: Generative modeling by estimating gradients of the data distribution. NeurIPS **32** (2019) [3](#)
58. Song, Y., Ermon, S.: Improved techniques for training score-based generative models. NeurIPS **33**, 12438–12448 (2020) [3](#)
59. Song, Y., Sohl-Dickstein, J., Kingma, D.P., Kumar, A., Ermon, S., Poole, B.: Score-based generative modeling through stochastic differential equations. arXiv preprint arXiv:2011.13456 (2020) [3](#)
60. Tang, S., Chen, C., Xie, Q., Chen, M., Wang, Y., Ci, Y., Bai, L., Zhu, F., Yang, H., Yi, L., et al.: Humanbench: Towards general human-centric perception with projector assisted pretraining. In: CVPR. pp. 21970–21982 (2023) [1](#), [4](#)
61. Tian, Y., Fan, L., Chen, K., Katabi, D., Krishnan, D., Isola, P.: Learning vision from models rivals learning vision from data. arXiv preprint arXiv:2312.17742 (2023) [1](#), [2](#), [4](#), [11](#), [14](#)
62. Tian, Y., Fan, L., Isola, P., Chang, H., Krishnan, D.: Stablerep: Synthetic images from text-to-image models make strong visual representation learners. In: NeurIPS (2023) [1](#), [2](#), [4](#), [7](#), [11](#)
63. Wei, C., Fan, H., Xie, S., Wu, C.Y., Yuille, A., Feichtenhofer, C.: Masked feature prediction for self-supervised visual pre-training. In: CVPR. pp. 14668–14678 (2022) [4](#)
64. Yuan, J., Zhang, X., Zhou, H., Wang, J., Qiu, Z., Shao, Z., Zhang, S., Long, S., Kuang, K., Yao, K., et al.: Hap: Structure-aware masked image modeling for human-centric perception. In: NeurIPS (2023) [1](#), [4](#), [5](#), [7](#), [9](#), [10](#), [11](#), [13](#), [16](#)
65. Yufei, X., Jing, Z., Qiming, Z., Dacheng, T.: Vitpose: Simple vision transformer baselines for human pose estimation. In: NeurIPS (2022) [16](#)
66. Zhang, L., Rao, A., Agrawala, M.: Adding conditional control to text-to-image diffusion models (2023) [2](#), [3](#)
67. Zheng, L., Shen, L., Tian, L., Wang, S., Wang, J., Tian, Q.: Scalable person re-identification: A benchmark. In: ICCV. pp. 1116–1124 (2015) [10](#), [11](#), [12](#), [17](#)
68. Zhu, A., Wang, Z., Li, Y., Wan, X., Jin, J., Wang, T., Hu, F., Hua, G.: Dssl: Deep surroundings-person separation learning for text-based person retrieval. In: ACM MM. pp. 209–217 (2021) [10](#), [11](#), [12](#), [17](#)